Novel double-layer core-shell photocatalyst CdS-TiO$_2$@NH$_2$-MIL-101: Enhanced conversion of CO$_2$ and CH$_4$ at ambient temperature

Yufei Huang,[a] Ling Tan,[a] Hanyu Ma,[b] Xuan Wang,[c] Yangqiang Huang,[*a] Jinping Yin,[c] Zhiwu Liang[*a] and Xiao Luo[*a]

[a]Joint International Center for CO$_2$ Capture and Storage (iCCS), The Engineering Research Center of Advanced Catalysis, Ministry of Education Provincial, Hunan Key Laboratory for Cost-effective Utilization of Fossil Fuel Aimed at Reducing CO$_2$ Emissions, College of Chemistry and Chemical Engineering, Hunan University, Changsha 410082, PR China.

[b]College of Chinese Language and Literature, Hunan University, Changsha 410082, PR China.

[c]Shanghai Yanlu Manman technology Co., LTD.

* Author for correspondence: Email: x_luo@hnu.edu.cn (Dr. Xiao Luo), zwliang@hnu.edu.cn (Dr. Zhiwu Liang)

Content

1. Materials

Iron (III) chloride hexahydrate ($FeCl_3.6H_2O$; 99%), 2-Aminoterephthalate (98%) and N, N-dimethylformamide (DMF; 99.9%) was obtained from Shanghai Aladdin Biochemical Technology Co. Ltd., China. Nitric acid (HNO_3; 65%), Tetra-n-butyl titanate (98%) and Anhydrous ethanol (99.7%) were purchased from Sinopharm Chemical Reagent Co. Ltd., China. The Dimethyl Sulfoxide and $Cd(OAc)_2 \cdot 2H_2O$ was purchased from Shanghai Aladdin Biochemical Technology Co. Ltd., China. Hydrogen (H_2; 99.9999%), Carbon dioxide (CO_2; 99.9999%), methane(CH_4; 99.9999%), Air (99.99%) and Argon (Ar; 99.9999%) were prepared by Changsha Jingxiang Gas Co. Ltd., China. The Labsolar-6A was obtained from Beijing Perfectlight Technology Co., Ltd, China. All materials were used without further purification.

2. Experiment method

2.1 preparation of TiO_2 quantum dots

TiO_2 quantum dots were synthesized by the wet chemical method, detailed experimental steps can be found in our previous research work[1].

2.2 Systhesis of CdS nanoparticle

The CdS was prepared by hydrothermal synthesis according to the literature with slight modification[2]. Firstly, 1.6 mmol of $Cd(OAc)_2 \cdot 2H_2O$ and 130 mL of Dimethyl Sulfoxide were added into a beaker. The mixed solution was uniformly stirred at room temperature for 30 minutes. Next, the above substances were quickly transferred to a hydrothermal reactor and heated in air at 180 °C for 12 h. The hydrothermal reactor was naturally cooled to room temperature, and the suspension obtained was filtered through a centrifuge and washed by ethanol and water three times each.

3. Characterization

The crystal structure and composition of the materials were discussed by X-ray powder diffraction using a Rigaku Ultima IV and XRD-600 with CuKa radiation ranging from 4° to 60° (4°-10°; 10°-60°), corresponding to a step of 0.5^o /min and 2° /min, respectively. The Fourier transform infrared spectra (FTIR) experiment was performed on a Vector 22 FT-IR to studied the molecular structure and chemical composition of samples. The N_2 adsorption-desorption data was recorded by Jw-bk200c, and determined the specific surface area and pore size distribution of photocatalysts with Brunauer-Emmett-Teller (BET) method and Barrett-Joyner-Halenda (BJH), respectively. The morphology and structure of hybrid materials were researched by scanning electron microscopy (SEM) and transmission electron microscopy (TEM) methods by JEM-2100 plus and JSM-6700F, respectively. The composition and chemical states of Composite material was evaluated by the X-ray photoelectron spectroscopy (XPS) Characterization methods, performing on an AXIS SUPRA. The light absorption ability of photocatalysts was explored by UV–vis diffuse reflectance spectra approach, taking out in a UV-2600 with a wavelength range of 200-800 nm. The DTG-60 was applied to research thermogravimetric analysis (TGA) of material. Photoluminescence (PL) spectra experiment was carried out on a fluorescence spectrometer, analyzing the optical responses of the photocatalysts.
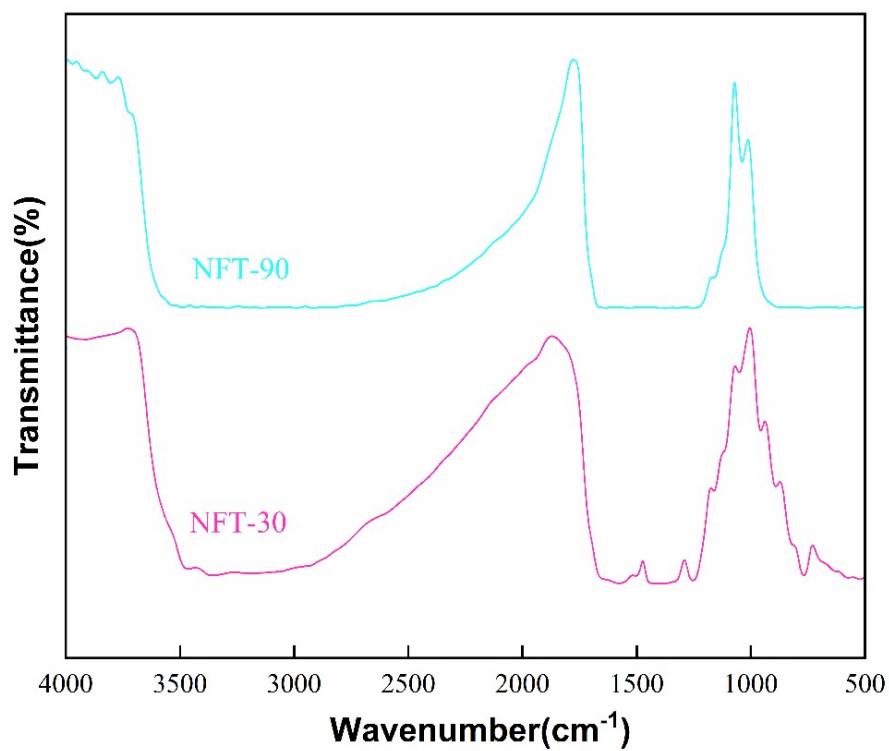
Figure S1. FT-IR spectra of TiO$_2$@NH$_2$-MIL-101 materials.
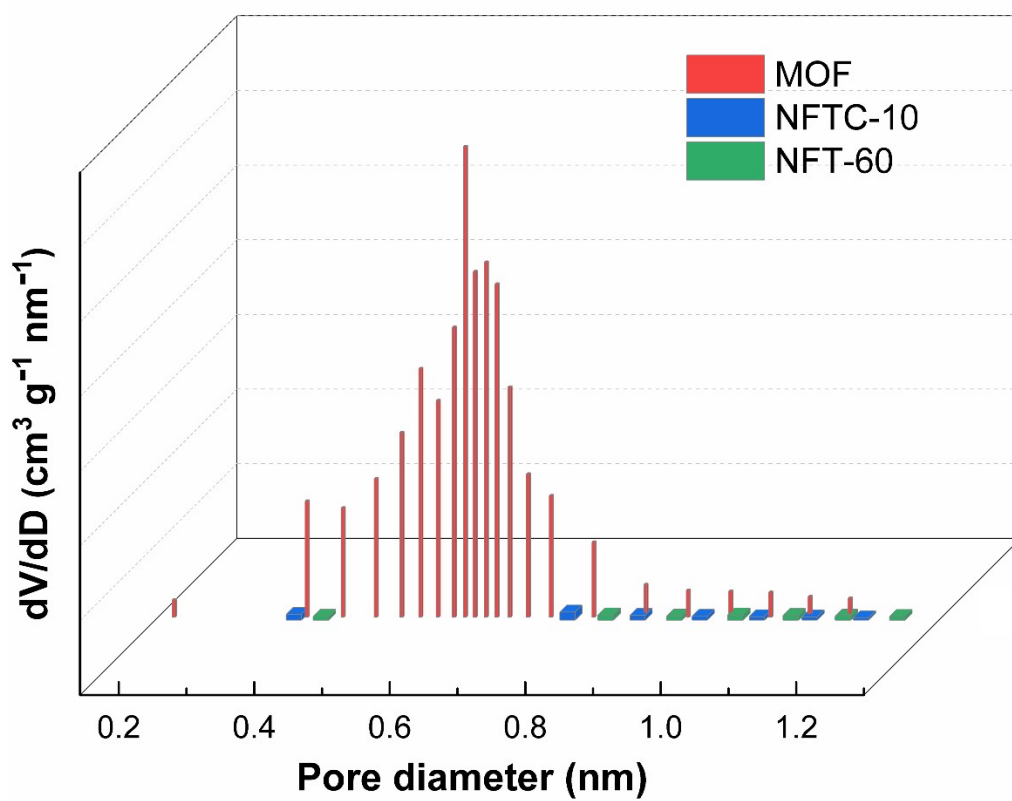

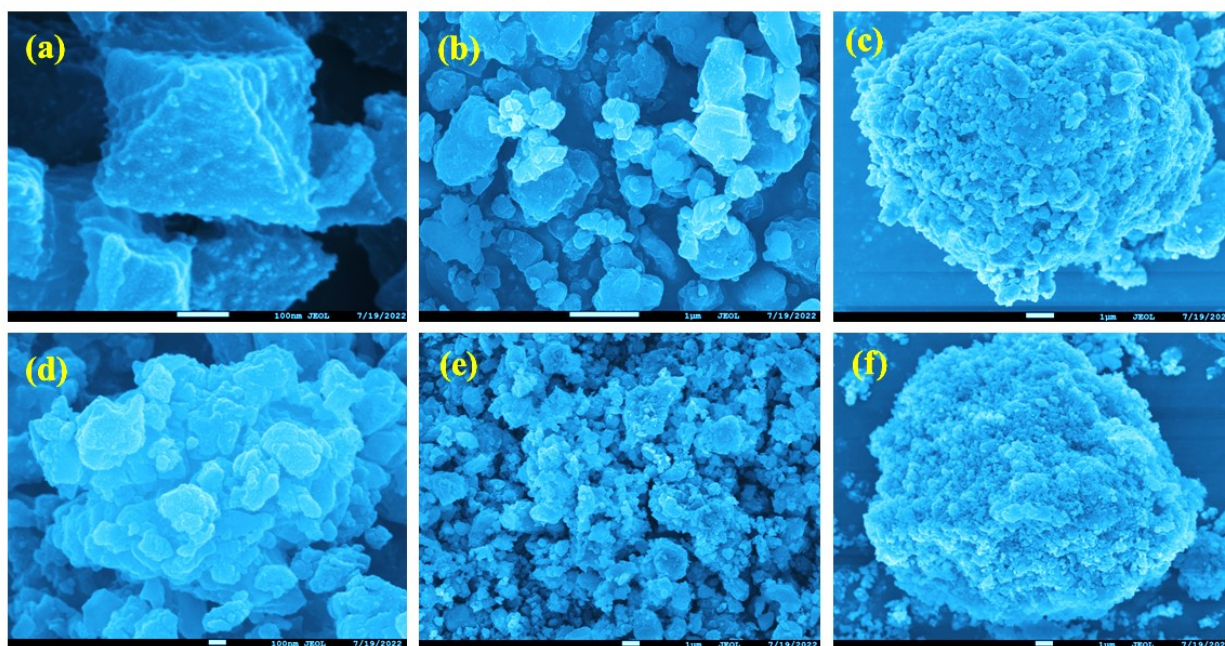**Figure S2.** Particle size distribution curves of different catalysts.

Figure S3. SEM images of catalysts: (a was MOF; b was NFT-30; c was NFT-60; d was NFT-90; e and f are NFTC-10).
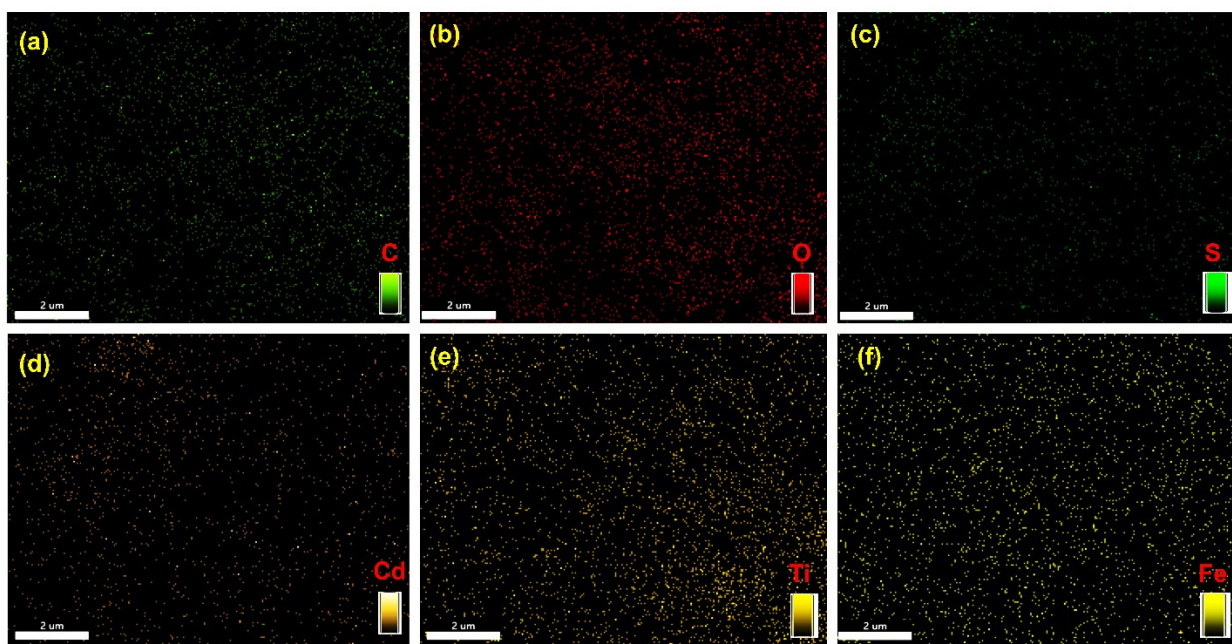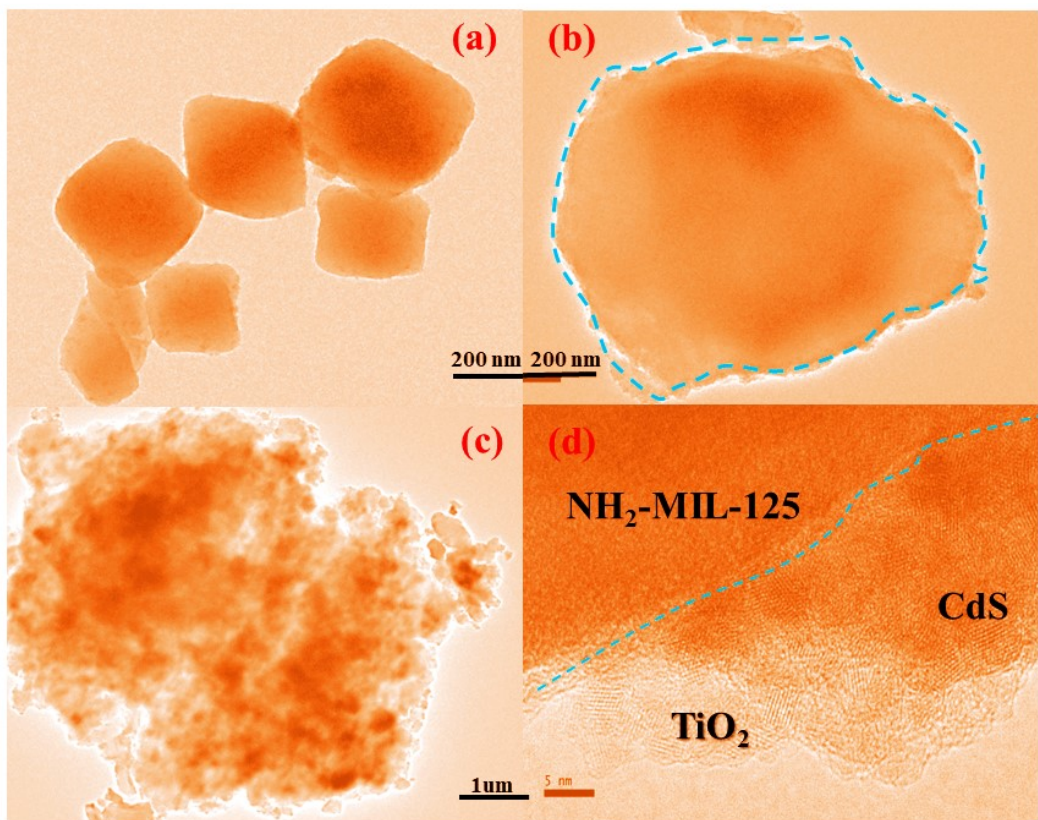

Figure S4. EDX mapping images of NFTC-10.

Figure S5. TEM pictures of the prepared samples ((a) was NH$_2$-MIL-101; (b) was NFT-30; (c) was NFT-30; (d) was HR-TEM images of NFTC-10).

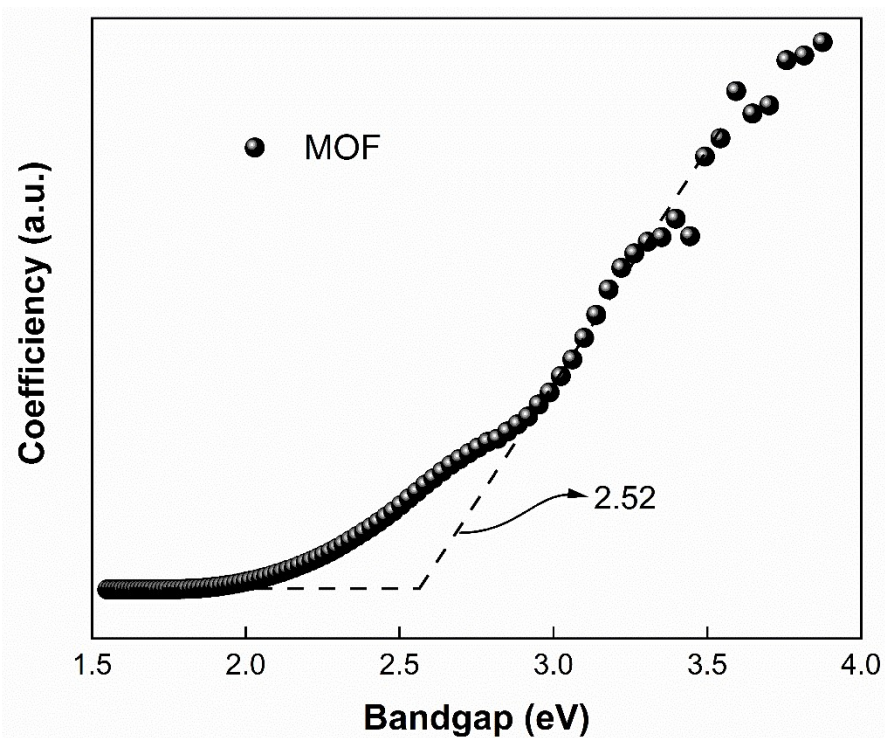**Figure S6.** Band gap energy of MOF, TiO$_2$@NH$_2$-MIL-101 and CdS-TiO$_2$@NH$_2$-MIL-101 catalysts.

4. Computational methods

All calculations in the paper were spin polarized and carried out with the Perdew–Burke–Ernzerhof (PBE)[3] functional in Vienna ab initio simulation package (VASP)[4, 5]. The D3 correction method[6] was employed in order to include van der Waals (vdW) interactions. The project-augmented wave (PAW) method was used to represent the core–valence interaction[7, 8]. For the calculations of total energy, a cut-off energy of 400 eV was set for plane wave basis sets to expand the valence electronic states, and the converging criteria of the force on each relaxed atom below 0.02 eV/Å was used for structural optimizations.

The adsorption energy (ΔG_{ad}) was defined as:

$$\Delta G_{ad} = G_{adsorbate+surface} - G_{adsorbate} - G_{surface} \qquad (1)$$

where $G_{surface}$, $G_{adsorbate}$, and $G_{adsorbate+surface}$ are the free energies of the surface, adsorbate in the gas phase, and adsorbate adsorbed on the surface, respectively. The free energy G is calculated from the total energy E (by DFT calculation) and thermal corrections (including zero-point energy ZPE, internal energy U, and entropy S):

$$G = E_{DFT} + ZPE + U - TS \qquad (2)$$

All thermal corrections are obtained by frequency calculations of VASP followed by VASPKIT data processing[9]. The transition states (TS) are determined by a constrained optimization scheme[10, 11], which are verified until (i) all forces on atoms vanish; and (ii) the total energy reaches maximum along the reaction coordination but minimum with respect to the rest of the degrees of freedom. All atoms are fully relaxed during optimization, and the Brillouin zone was sampled as $2 \times 2 \times 1$ for both surfaces.
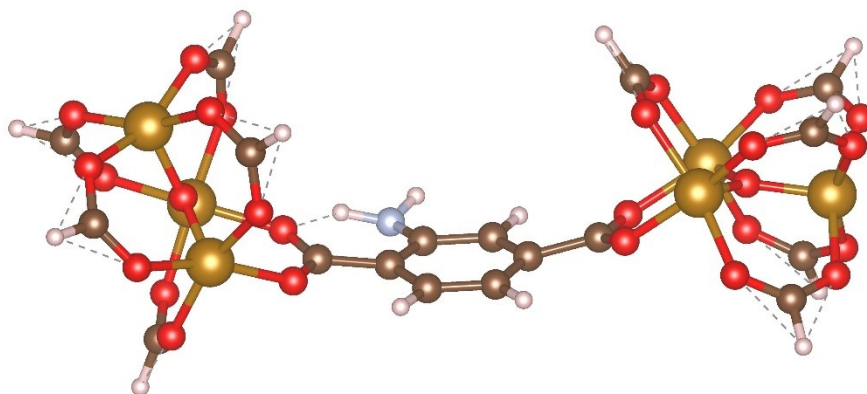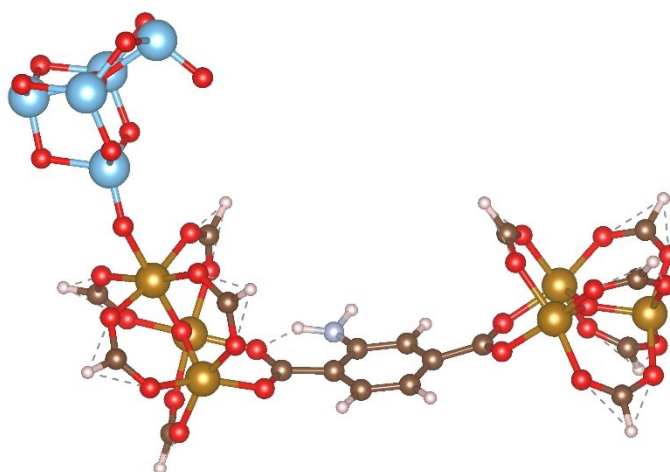
Figure S7. Model diagram of NH$_2$-MIL-101 (Fe).
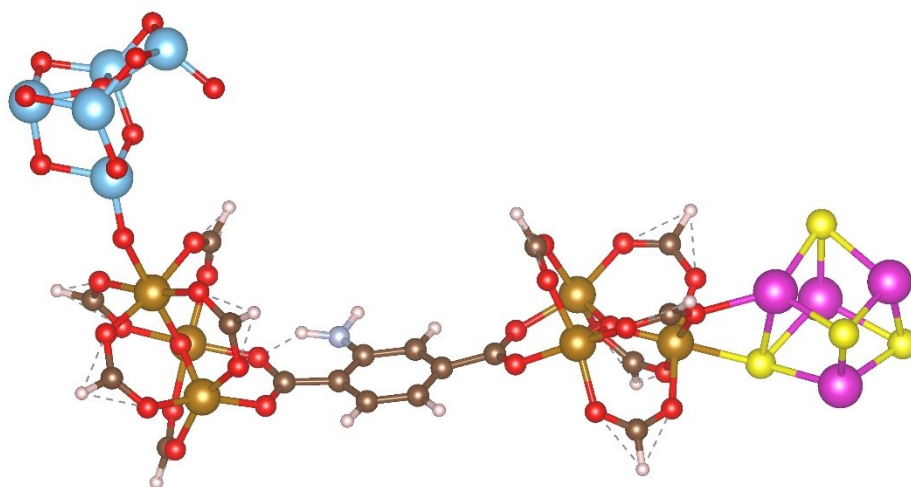

Figure S8. Model diagram of TiO$_2$@NH$_2$-MIL-101 (Fe).
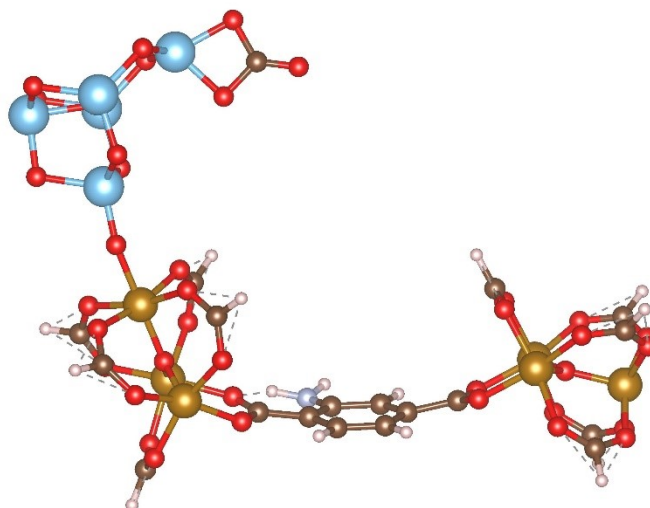
Figure S9. Model diagram of CdS-TiO$_2$@NH$_2$- MIL-101 (Fe).

Figure S10. Adsorption model of CO$_2$ by TiO$_2$@NH$_2$- MIL-101 (Fe).
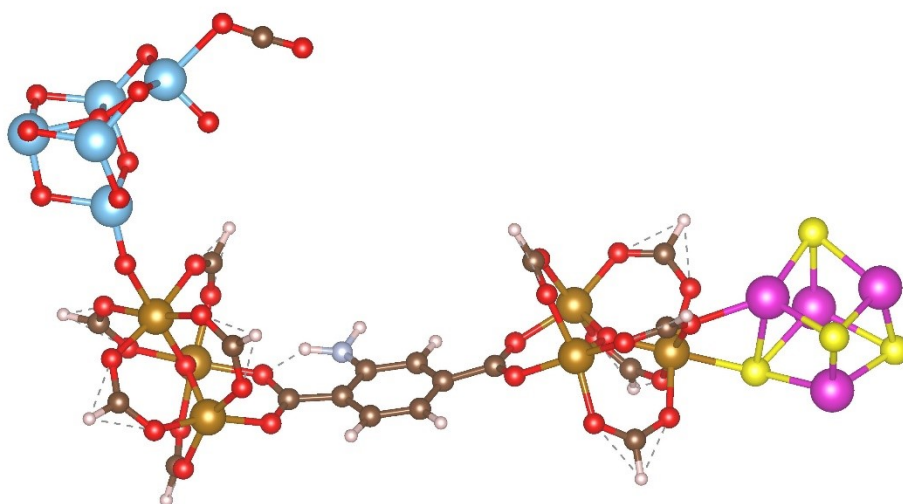
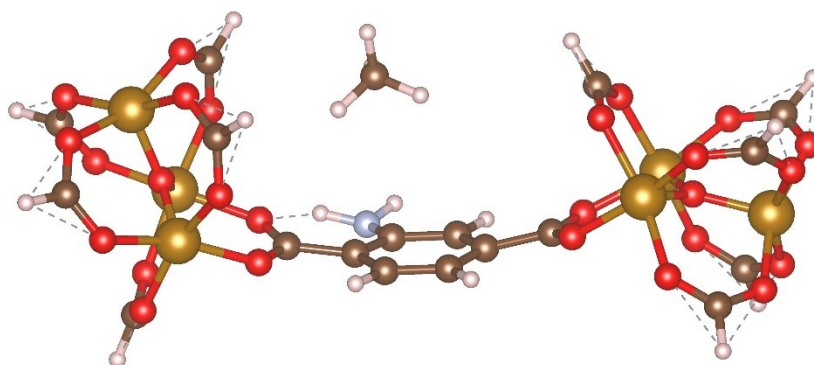**Figure S10. Adsorption model of CO_2 by CdS-TiO$_2$@NH$_2$- MIL-101 (Fe).**

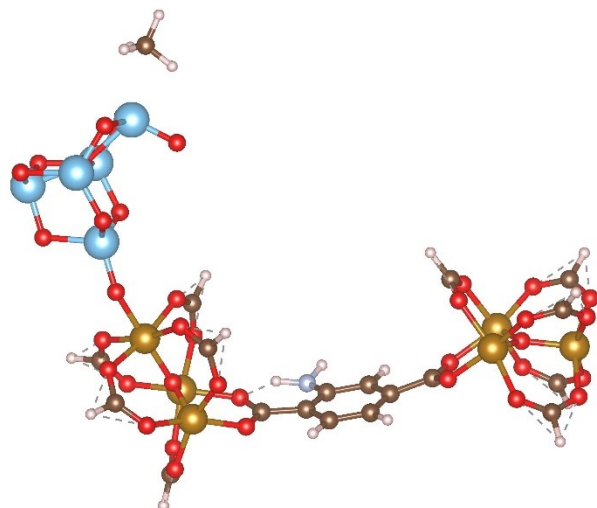**Figure S11. Schematic diagram of the model of NH$_2$- MIL-101 (Fe) activation of CH_4.**

Figure S12. Schematic diagram of the model of TiO$_2$@NH$_2$- MIL-101 (Fe) activation of CH$_4$.

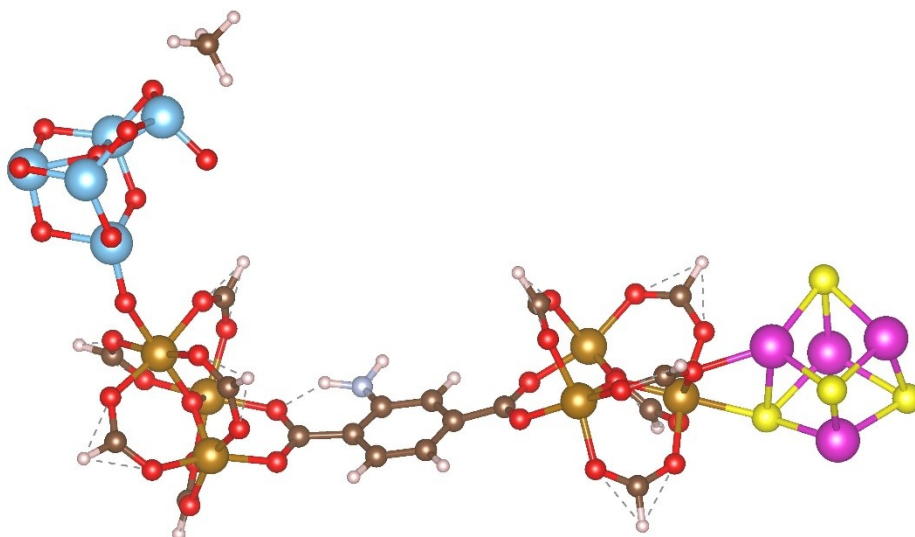**Figure S13. Schematic diagram of the model of CdS-TiO$_2$@NH$_2$- MIL-101 (Fe) activation of CH$_4$.**

Reference

1.   Y. Huang, D. Wei, Z. Li, Y. Mao, Y. Huang, B. Jin, X. Luo and Z. Zhi, *Sep. Purif. Technol.* 2023, 123174.

2.   J. Thote, H. B. Aiyappa, A. Deshpande, D. Diaz Diaz, S. Kurungot and R. Banerjee, *Chem. Eur. J.* 2014, **20**, 15961-15965.

3.   J. P. Perdew, K. Burke and M. Ernzerhof, *Phys. Rev. Lett.*, 1996, **77**, 3865-3868.

4.   G. Kresse and J. Furthmüller, *Comput. Mater. Sci.*, 1996, **6**, 15-50.

5.   G. Kresse and J. Hafner, *Phys. Rev. B*, 1994, **49**, 14251-14269.

6.   J. Klimeš, D. R. Bowler and A. Michaelides, *Phys. Rev. B*, 2011, **83**.

7.   G. Kresse and D. Joubert, *Phys. Rev. B*, 1999, **59**, 1758-1775.

8.   P. E. Blöchl, O. Jepsen and O. K. Andersen, *Phys. Rev. B*, 1994, **49**, 16223-16233.

9.   V. Wang, N. Xu, J. Liu, G. Tang and W. Geng, *Preprint at https://arxiv. org/abs/1908.08269*, 2019.

10.   A. Alavi, P. Hu, T. Deutsch, P. L. Silvestrelli and J. Hutter, *Phys. Rev. Lett.*, 1998, **80**, 3650-3653.

11.   Z.-P. Liu and P. Hu, *J. Am. Chem. Soc.*, 2003, **125**, 1958-1967.